Influence of defects on the tensile behaviour of flax fibres: Cellulose microfibrils evolution by synchrotron X-ray diffraction and finite element modelling

E. Richely, L. Nuez, J. Pérez, C. Rivard, C. Baley, A. Bourmaud, S. Guessasma, Johnny Beaugrand

Composites Part C: Open Access 9 (2022) 100300

Contents lists available at ScienceDirect

Composites Part C: Open Access

journal homepage: www.sciencedirect.com/journal/composites-part-c-open-access

Influence of defects on the tensile behaviour of flax fibres: Cellulose microfibrils evolution by synchrotron X-ray diffraction and finite element modelling

E. Richely [a], L. Nuez [b,c], J. Pérez [d], C. Rivard [d,e], C. Baley [c], A. Bourmaud [c], S. Guessasma [a], J. Beaugrand [a,*]

[a] UR1268 Biopolymères Interactions Assemblages, INRAE, Nantes, France
[b] Van Robaeys Frères, Killem, France
[c] Univ. Bretagne Sud, UMR CNRS 6027, IRDL, Lorient, France
[d] Synchrotron SOLEIL, Heliobio team, SWING-LUCIA beamlines, Gif-sur-Yvette, France
[e] UAR 1008 TRANSFORM, INRAE, Nantes, France

ARTICLE INFO

Keywords:
Agrocomposites
Microfibril angle
Dislocations
Tensile behaviour
Finite element analysis

ABSTRACT

The cellulose microfibril realignment of unitary flax fibres with contrasted density of structural defects, which are also known as dislocations and defined as zones of microstructure heterogeneities, was investigated upon tensile testing by means of X-ray diffraction performed on SWING beamline at synchrotron SOLEIL. The *in situ* continuous tensile tests demonstrate a microfibril angle (MFA) decrease ranging from 3 to 24% depending on the fibre, with initial MFA measured between 4.7° and 7.4°. The correlation between both the initial and final MFA values and the defect density is further assessed thanks to polarized light microscopy measurements prior to tensile testing. The influence of twisting and initial orientation of the fibres are also highlighted and discussed. Both the heterogeneity of the MFA values along flax fibres and the cellulose microfibril reorientation upon stretching are evidenced by stepwise tensile testing with an X-ray beam vertical size reaching 20 μm. Indeed, initial MFA values vary between 4.5 and 17° along the fibres observed. The results are implemented in a finite element model in the elastic domain based on precise fibre morphologies obtained by X-ray microtomography. The numerical results quantify the influence of the microfibril realignment on the resulting apparent modulus, with a stiffening between 1.5 and 7.5% only partly explaining the non-linearities observed experimentally.

1. Introduction

In the present context of growing environmental concerns, the energy-intensive production of most synthetic fibres combined to end-of-life issues in composites applications have been driving the development of alternatives. The expansion of plant-based biocomposites for structural applications requires a better knowledge of the structure-property relationship within plant fibres, and especially flax due to its high potential [1]. In particular, the cellulose microfibril orientation and its effect on the mechanical properties demand extensive investigation.

Plant fibres can be seen as composite materials where cellulose crystalline microfibrils backboned with semi-crystalline areas reinforce a surrounding matrix made of amorphous polysaccharides, mainly hemicelluloses, pectins and lignin to a lesser extent [2]. Flax fibres are multinucleate cells of high aspect ratio (a few centimetres in length for a diameter of 10 – 30 μm [3]), which are mechanically extracted from the stems by scutching and hackling processes [4]. After the mechanical extraction, the individualization is only partial and the fibres remain in the form of bundles, i.e. few tens of fibres glued together by a pectin rich interphase called the middle lamella [5, 6]. At the fibre scale, the flax cell wall is divided in four layers: the primary cell wall and secondary cell wall that is further divided between the S1, G and Gn layers [7–9]. The thickest gelatinous G layer, representing 5 – 10 μm in thickness [10], is formed from the progressive conversion of the Gn layer [11]. The fibres present a main internal porosity called lumen and representing up to 7% of the total fibre volume [12]. Therefore, both the orientation, crystallinity and amount of cellulose in the different sublayers (and especially in the main G-layer), as well as the porosity content; are

* Corresponding author.
E-mail address: johnny.beaugrand@inrae.fr (J. Beaugrand).

https://doi.org/10.1016/j.jcomc.2022.100300

Available online 30 July 2022

important parameters influencing the mechanical properties of the fibres [1, 6]. The overall cellulose content reported in the literature varies between 50 and 90% [13]. Moreover, Bourmaud et al. [14] observed a crystallinity rate between 52 and 56% on flax by NMR (Nuclear Magnetic Resonance) depending on the retting degree. In the main G-layer, the cellulose microfibrils, with diameters between 2 and 4 nm [14, 15], form Z-helix along the fibre cell walls, with a particular angle φ called the MFA (Fig. 1). Down to the supramolecular scale, cellulose microfibrils are predominantly made of β-(1–4)-D-glucopyranose chains, which are assembled by hydrogen bonds between hydroxyl groups and van der Waals interactions in generally accepted 24 or 36 chains model to form cellulose I_β [16]. The resulting crystal unit cell is monoclinic, with the following unit cell characteristics: $a = 7.84$ Å, $b = 8.20$ Å and $c = 10.38$ Å and $\gamma = 96.5°$.

X-ray diffraction (XRD) is a widespread technique to assess the crystallographic structure, phases, sizes, preferred orientation or chemical composition of crystalline materials. For plant fibres, XRD appears as a reliable method to determine the microfibril angle of crystalline cellulose with the advantage of requiring no pre-treatment and being statistically reliable. The technique is based on Bragg's law, enabling the determination of the diffraction conditions leading to constructive interferences within a material containing periodic structures:

$$n\lambda = 2d_{hkl} * \sin\theta \quad (1)$$

where λ is the X-ray wavelength, 2θ is the angle between the incident beam and the diffracted beam, d_{hkl} is the periodic distance within the sample and n is an integer. The diffraction planes, defined by the incident beam and the diffracted beam, include the direction of the related structural periodicity. The alignment of the microfibrils with respect to the fibre axis can therefore be measured. Compared to XRD, experimental characterization of MFA by Atomic Force Microscopy, Scanning Electron Microscopy (SEM) or second-harmonic generation (SHG) microscopy rather correspond to the angle between the fibre axis and a bundle of microfibrils: the macrofibril [17]. Among diffraction techniques, one can distinguish Small Angle (SAXS) and Wide Angle (WAXS) X-ray Scattering depending of the range of wave vector observed. With WAXS, the MFA is usually measured from the width of the (200) reflection, representing the planes parallel to the microfibrils [18], or using a combination of the (200) and (004) reflections, thanks to different curve fitting or variance methods [19, 20]. With SAXS, the equatorial streak width can also lead to a MFA measurement, as well as microfibril diameters [21]. Several authors exploited X-ray diffraction techniques to measure the MFA of different plant fibres, and especially flax, as summarized in Table 1. Bourmaud et al. [22] reported MFA values for flax fibre bundles between 9.5 and 8.3°. Slightly lower values, between 7.2 and 6.2° were measured on oleaginous and textile flax fibre bundles by Wang et al. [23], in good agreement with SEM observations. Astley and Donald [24] measured the MFA of flax at the fibre bundle scale between 5.5 and 7.5° depending on the hydration level using SAXS. The orientation of the cellulose microfibrils is believed to play a significant role in the complex mechanical behaviour of plant fibres [25–27]. Experimental validation was obtained by Keckes et al. [28] on wood foil and fibres, showing a decrease of MFA correlated to the tensile strain: the cellulose microfibrils were compared to springs. Placet et al. [18] studied the MFA evolution during a stepwise tensile test on hemp fibre bundles by WAXS. They evidenced a non-linear decrease of the MFA, from 10.8 to 7.8° between 0 and 2% strain, distinguished into 3

Table 1
MFA values determined for different plant fibres by several authors and related experimental parameters.

Author	Fibre type and scale	MFA	Tensile testing	XRD technique
Wang et al. [23]	Oleaginous and textile flax fibre bundles	6.2° – 7.2°	No	WAXS
Bourmaud et al. [22]	Flax fibre bundles	8.3° – 9.5°	No	WAXS
Astley and Donald [24]	Flax fibre bundles, different hydration levels	5.5° (dry) – 7.5° (wet)	No	SAXS
Astley and Donald [30]	Flax fibre bundles	–	Yes	SAXS and WAXS
Müller [21]	Flax fibre + water	3.5°	No	μSAXS
Müller [37]	Flax fibre	5.3° – 6.4°		SAXS + WAXS
Kölln [31]	Flax and wood fibres	-	Yes	WAXS
Thuault [63]	Flax fibres	–	Yes	WAXS
Placet et al. [18]	Hemp fibre bundles	10.8°	Yes + cyclic loading	WAXS
Placet et al. [75]	Hemp fibre bundles	8° – 11.2°	No	WAXS
Martinschitz et al. [29]	Coir fibre bundles	45°	Yes + cycling loading	WAXS

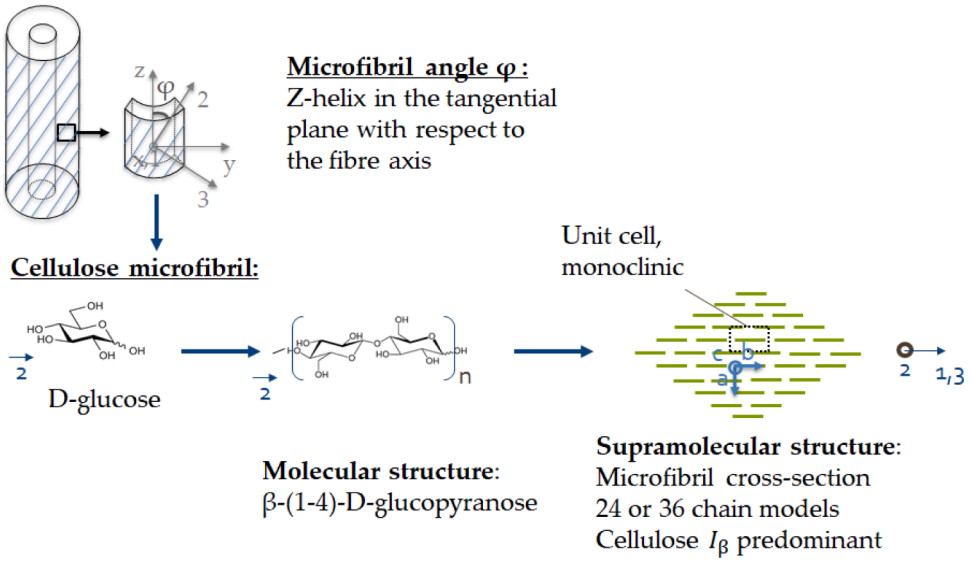

Fig. 1. Hierarchical organization of the cellulose microfibrils in the plant cell wall main G layer.

phases correlated to the rigidity variations observed for the stress-strain response. The MFA evolution of coir fibre bundles under quasi-static and cyclic tensile loading was studied using WAXS by Martinschitz et al. [29]. They reported a decrease of MFA upon increasing strain, with a partial recovery of the initial MFA upon unloading. Finally, both SAXS and WAXS measurements were performed by Astley and Donald [30] on flax fibre bundles during in situ tensile testing. The authors concluded on the absence of MFA reorientation upon loading and a strain-induced crystallisation of initially orientated amorphous cellulose microfibrils. These contradictory results were re-analysed and by Kölln et al. [31], who found a decrease of MFA of about 15% at 1% strain and ruled out the strain-induced crystallization scenario.

Laboratory facilities enable determination of the apparent MFA at the fibre bundle scale, with the related strong hypothesis of a homogeneous microfibril orientation. X-ray microbeam measurements at the unitary fibre, available on synchrotron beamlines, allow considering cell-wall inhomogeneities such as defects. Indeed, strong misalignment of the cellulose microfibrils from flax fibres have been observed in zones also known among others as defects, dislocations, kink bands or spots of micro-compressions [13, 32], with different severities and local microfibril angles (MFA) up to 47° reported by SHG microscopy by Melelli et al. [17]. Such defects appear when the fibre walls are subjected to uniaxial compression in the direction of the fibres. According to Thygesen et al. [33] defects creation could occur during the growth of the fibres subjected to environmental stresses. However, recent works converge towards defining the mechanical extraction of fibres from the bundles as the critical step of defect creation [34–36]. The consequence of defects in terms of mechanical properties and evolution upon tensile testing require *in situ* investigations that are scarce in literature. It remains a moot point [13] of interest to decipher in order to expand the use of plant fibres for structural applications in the field of biocomposites. Indeed, up to now, very few studies have been focusing on the MFA heterogeneities in the cell wall during a mechanical test because of the restricted access to the synchrotron and of the high acquisition speed required to perform *in situ* tensile testing. The MFA heterogeneities along a flax fibre and MFA evolution during a tensile test were evidenced by Kölln et al. [9] using WAXS. With an X-ray microbeam focused down to 2 μm and a step-wise tensile test, the authors highlighted inhomogeneities within the fibres and a tendency to a higher orientation for the initially less orientated areas with increasing strain. They also reported a decrease of microfibril angle between 10 and 20% depending on the fibre at 1% strain during continuous *in situ* tensile testing. Müller et al. [21] reported a mapping of a flax unitary fibre by μ-SAXS measurements after swelling in water to enhance the scattering contrast between amorphous and crystalline cellulose. They determined a mean MFA of 3.5° with variations along a flax unitary fibre. Higher values close to 6° were reported at the fibre edges, which could be attributed to less confident data such as the presence of an additional signal caused by refraction effects. A combined μ-SAXS/μ-WAXS setup was also implemented by the authors in another study on flax unitary fibre [37], leading to MFA measurements between 5.3 and 6.4° depending of the diffraction spot investigated (from SAXS strike or planes $(1\bar{1}0)$, (110) or (200)).

Numerical modelling appears as a complementary tool to investigate the consequences of microstructural organization on the mechanical performances, especially in ranking the contribution of structuring levels and testing the relevance of supposed deformation mechanisms. In the research field of plant fibres, a few analytical or Finite Element (FE) models have been taking into account the MFA [27, 38–43], and even fewer attempted to model defects as MFA heterogeneities along the fibres [44, 45]. In addition, meshless methods such as molecular dynamics have proven their ability to decipher mechanisms involving different MFA at the cell wall scale [46] and defects at the scale of the cellulose chains [47, 48]. However, most models were lacking accurate experimental data as inputs, more specifically those related to the microstructural evolution under mechanical loading.

The aim of the study is to better understand the complex tensile behaviour of flax fibres and the contribution of microfibril realignment, especially in defected areas. Indeed, up to our knowledge the direct link between defects and microfibril angle changes upon tensile testing was never assessed before. In the present study, the microfibril orientation of a contrasted panel of fibres in terms of defect density was therefore measured during *in situ* tensile testing by X-ray diffraction experiments on the SWING beamline at Synchrotron SOLEIL. Measurements were achieved at different locations along fibres to assess the microfibril angle heterogeneities. The results were further implemented in a FE model to quantify the effect of realignment upon tensile loading and MFA heterogeneities along fibres on the mechanical properties.

2. Material and methods

2.1. Materials

Textile flax fibres *(Linum usitatissimum)* from the Bolchoï variety were provided by Groupe Depestele / Teillage Vandecandelaère (Bourguebus, France). The plants were cultivated in 2017 in Normandy (France), dew-retted in the field and scutched on an industrial facility following the standard chain of fibre extraction [49]. In addition, the scutched fibres were deliberately damaged by numerous additional passages between fluted rollers on a pilot scutching line at ENIT (Tarbes) [50]. Fibre extraction was achieved by hand from the middle section of the scutched fibres.

2.2. Optical microscopy

Optical images were obtained using a microscope (Leitz DMRB, Leica Microsystems, Nanterre, France) equipped with a Hamamatsu digital camera (C11440 ORCA-Flash4.0 LT). High resolution image scanning was performed thanks to a motorized stage (Marzhauser), allowing a 15 mm scanning along the fibres glued on a 15 mm cardboard frame. Images were acquired using both bright light and a linearly polarized light with an optical objective x20, leading to a maximum spatial resolution of 49,000 × 2000 pixels, with a pixel size of 328 nm. Image processing of the polarized light scans was conducted using FIJI software (https://fiji.sc/) in order to determine the surface area of defects which appear as bright areas under polarized light [51]. The same threshold was applied to all images. Each resulting binary image and initial grey-scale image were compared to check the accuracy of the result. The proportion of defects along each fibre is defined as follow:

$$p\ (\%) = 100 * \frac{S_d}{S_f} \tag{2}$$

Where S_d is the cumulative surface area of defects resulting from image processing, and S_f is the fibre surface area. The latter was estimated from the mean diameter, calculated from 6 measurements along each fibre multiplied by the image length.

2.3. Tensile testing

- Reference tensile testing

42 unitary fibres from the Bolchoï variety were tensile tested using a MTS machine (MTS System, Créteil, France). The testing parameters were the following: a 2 N load cell, a displacement rate of 1 mm/min and a controlled environment of 25 ± 1 °C and 48 ± 2% of relative humidity. The fibres were extracted manually from the middle part of the bundles and glued on a cardboard frame with a gauge length of 10 mm following the standard AFNOR NF T 25–501–2 and enabling comparison with literature data. Finally, the compliance of the system was considered in the calculations to compensate the influence of non-specimen

extension in tensile testing leading to an under-estimation of Young's modulus (E) and over-estimation of strain [52].

- *In situ* tensile testing

Tensile testing experiments were carried out during X-ray measurements on unitary fibres using a Linkam machine TST350 (Linkam Scientific Instruments, Epsom, UK) with a 20 N load cell and a 15 mm gauge length due to technical specifications of the machine (Fig. 2). The fibres were glued on cardboard frames prepared by laser cut and adapted for optimal fibre alignment on the tensile bench. Moreover, laser markings were placed at intervals of 0.5 mm in the 5.5 mm central zone accessible to X-ray measurement to recall specific locations of interest noticed during optical scanning (Fig. 2b). The environment was recorded thanks to a unified humidity-temperature sensor placed close to the jaws, with temperature and relative humidity values of respectively 25.5 ± 1.5 °C and 42 ± 7%. Both continuous and stepwise tensile tests were conducted with a displacement rate of 1 mm/min corresponding to a strain rate of 6.7% / min. For the stepwise tensile tests, displacement increments of 30 – 60 μm were employed.

For both tensile testing experiments, the cross-sectional areas are needed to calculate the resulting stress and Young's modulus and were determined under the assumption of cylindrical cross-section, and the mean diameter was obtained from 6 measurements along each fibre [53] using the optical microscope described in 2.2.

2.4. X-ray diffraction

X-ray diffraction experiments were performed on the SWING beamline of SOLEIL Synchrotron radiation facility (Gif-sur-Yvette, France). The overall set-up is displayed on Fig. 2a. The X-ray beam was set to an energy of 15 keV. A diamond active beam-stop recently developed by Desjardins et al. [54] was used for stopping the direct beam. The CCD detector of 1032 × 1088 pixels (77.4 × 81.6 mm) was placed at 520 mm from the sample, allowing to obtain a quarter of the diffraction pattern with q value up to 2.03 $\AA^{-1}$ (Fig. 2c). The tensile machine was placed on two translating tables, allowing 1 μm precision on the displacements in the horizontal (X) and vertical (Z) directions. Three different settings were used in the experiment (Fig. 3): 1) a continuous tensile testing at a single location along the fibres positioned horizontally, with acquisition times ranging from 160 to 600 ms and a X-ray beam size of 250 × 20 μm^2 – 550 × 20 μm^2; and stepwise tensile testing allowing a mapping along the fibres, with an X-ray beam length of 250 × 20 μm and fibres positioned 2) horizontally and 3) vertically. The displacement was applied at both clamping ends. In the case of setting 1, the X-ray beam of 250 μm in length was focused in the middle of the fibres, therefore the assumption of negligible fibre translation was made. In the case of settings 2 and 3, as the 5 mm central part of the 15 mm-fibre was scanned by XRD, the uncertainties regarding fibre translation upon tensile testing are more important, estimated to a maximum absolute value of 35 μm and 10 μm, respectively (one third of the maximum displacement applied at each fibre edge).

As the fibres were not naturally perfectly straight and not perfectly horizontally or vertically fixed on the cardboard frames, a crucial point is to place the centre of fibre on the X-ray beam and assess the related error on the MFA measurements. Therefore, jaws displacements of 10 μm were applied to each fibre prior to the tensile test until reaching an initial force of 0.01 N to ensure a straight fibre. XRD measurements were then recorded during transversal scan of the fibre to determine the centre of the fibre for the acquisition, as displayed in Fig. 4, showing an optimal Z-position corresponding to the maximum signal azimuthal integration intensity around 20 – 25 μm, and a related error on the MFA estimated to 0.5° for the rest of the experiments.

The software ***Foxtrot*** developed by Synchrotron SOLEIL was used for data analysis. Several diffraction spots could be analysed on the diffraction pattern (Fig. 2c). The (200) reflection was selected as it provides a high signal to noise ratio with sufficient counting statistics and no overlapping with other diffraction spots, in agreement with the method described by several authors [18, 22, 55, 56].

The inter-plane distance d_{200} is linked to the diffusion vector Q_0 by:

$$d_{200} = \frac{2 * \Pi}{Q_0} \tag{3}$$

where Π≈ 3.14159.

The first step involved the masking of the blank pixels between the detector frames and beam stop on the diffraction patterns. Then, a first radial integration of the intensity was conducted on the masked diffraction pattern (Fig. 2c). A Gaussian curve fitting using the following equation was realized to determine the optimal Q_0 corresponding to the maximum intensity of the (200) plane:

$$f(x) = A\exp\left(-\frac{(x-Q_0)^2}{2\sigma^2}\right) + Bx + C \tag{4}$$

where A, B, and C are constants determined from the fitting routine.

At this particular Q_0, a second integration of the azimuthal profile was achieved (Fig. 2c). The resulting Half Width at Half Maximum (HWHM) of a Gaussian curve fitting is estimated from the standard deviation σ through the following equation:

$$HWHM \simeq 1.178 * \sigma \tag{5}$$

The HWHM, referred to as the MFA, provides an estimation of the microfibril orientation. However, it should be mentioned that this common method used to estimate a mean MFA based on the curve fitting analysis of the reflection (200) depends on the shape of the fibre [19]. As the geometries of flax fibres usually differ from one to another and along their length [12], the calculation method induces uncertainties. More sophisticated methods, involving the complementary use of the reflections (200) and (004) for instance [57], can be used to improve the reliability of the data and estimate the shape of the cells. However, the (004) reflection was not usable (Fig. 2c) in our case as it requires

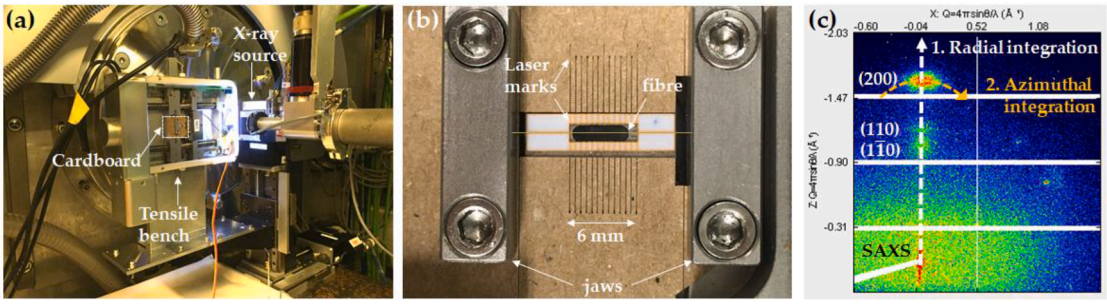

Fig. 2. (a) Experimental set-up on SWING beamline, (b) Zoom on the cardboard frame design mounted on the tensile bench, (c) Diffraction pattern of a flax unitary fibre and schematic representation of the two integrations involved in the data processing of the (200) diffraction spot.

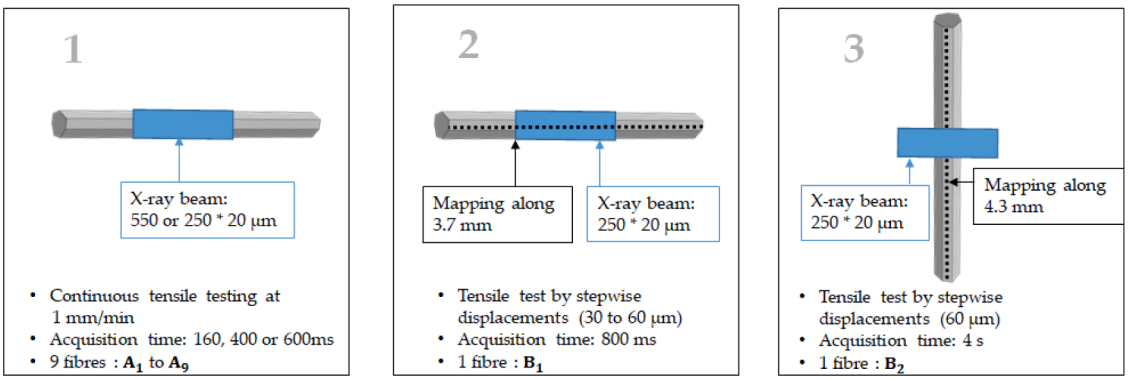

Fig. 3. The three different settings used for XRD experiments. N.B.: the length of the fibre is minimized in this schematic representation in order to visualize correctly the X-ray beam.

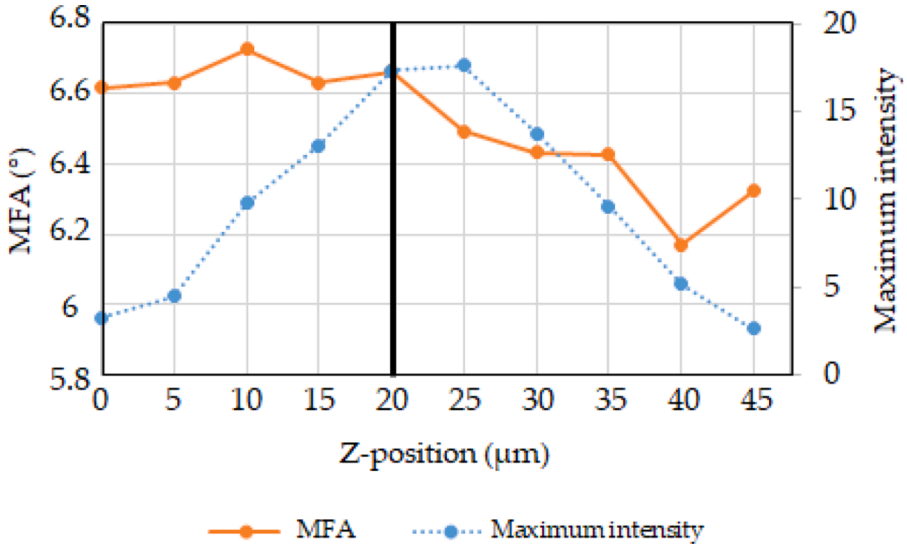

Fig. 4. Microfibril angle and azimuthal intensity calculated on a unitary fibre for different X-ray beam vertical position (setting 1). The black vertical bar represents the z-position chosen for further acquisition.

significantly altering the setup. The present values remain of interest for comparison purposes as it is the case in the present article.

Following tensile testing, the realignment is calculated using Eq. (6), with MFA_i and MFA_f the microfibril angles calculated respectively immediately after the pretension stage (i) and just before the fibre failure (f):

$$\text{Realignment}(\%) = 100 * \frac{MFA_i - MFA_f}{MFA_i} \quad (6)$$

2.5. Numerical model

Three different numerical models were built in order to i) assess the influence of the MFA on Young's modulus depending on the porosity content (lumen) using fibre models, ii) quantify the evolution of Young's modulus upon microfibril realignment at a single location along two contrasted fibres in terms of defect content and MFA initial values and realignment upon tensile testing (called thereafter **A4** and **A5**) analysed

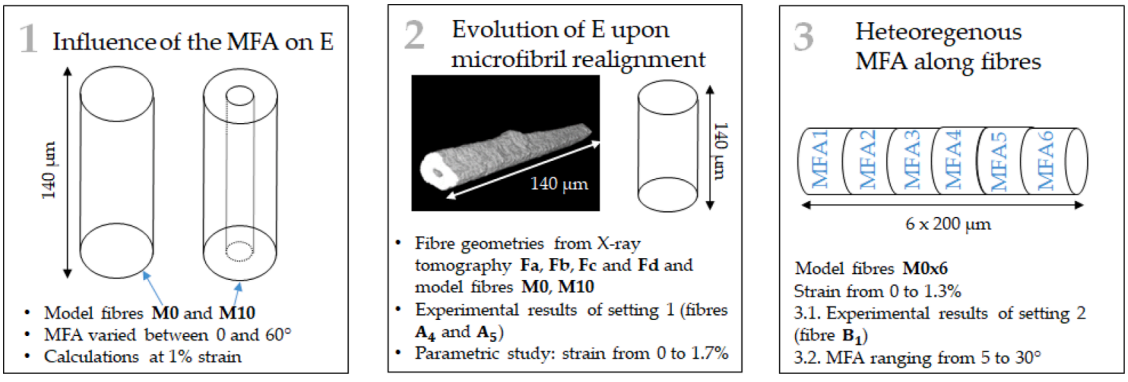

Fig. 5. Details of the considered finite element models used in the study.

on SWING beamline, and iii) consider the heterogeneous microfibril orientations along a fibre (called thereafter $\mathbf{B}_1$) analysed on SWING beamline and a second scenario with initial MFA ranging between 5 and 30° (fibre models). The main parameters of the models are summarized in Fig. 5 and details of the fibre geometry and meshing are summarized in Table 3. The model was based on precise geometry of fibres obtained by X-ray microtomography and compared to cylindrical fibre approximation without taking into account the MFA in previous studies conducted by the team [50, 58].

The material is considered elastic, neglecting viscous and plastic contributions. Therefore, following Hooke's law:

$$[\sigma] = [S^e]^{-1} * [\varepsilon] = [C^e] * [\varepsilon] \tag{7}$$

and

$$[\varepsilon] = [S^e] * [\sigma] \tag{8}$$

Where [σ] is the stress matrix (3 × 3), [ε] the strain matrix (3 × 3), [S] the tensor of compliance and [C] the stiffness tensor. In the local coordinate system related to the cellulose microfibrils (1,2,3) (Figs. 1, 6), the direction of the microfibrils is an axis of symmetry, and the fibre cell wall can be seen as a transverse isotropic material. Therefore, the elastic compliance tensor is the following:

$$[S^{e*}] = \begin{bmatrix} \frac{1}{E_T} & -\frac{\nu_{TT}}{E_T} & -\frac{\nu_{TL}}{E_T} & 0 & 0 & 0 \\ -\frac{\nu_{TT}}{E_T} & \frac{1}{E_T} & -\frac{\nu_{TL}}{E_T} & 0 & 0 & 0 \\ -\frac{\nu_{LT}}{E_L} & -\frac{\nu_{LT}}{E_L} & \frac{1}{E_L} & 0 & 0 & 0 \\ 0 & 0 & 0 & \frac{1}{G_{LT}} & 0 & 0 \\ 0 & 0 & 0 & 0 & \frac{1}{G_{LT}} & 0 \\ 0 & 0 & 0 & 0 & 0 & \frac{1}{G_{TT}} \end{bmatrix} \tag{9}$$

where E_L and E_T are the longitudinal and transverse Young's moduli of the cell wall, G_{LT} and G_{TT} are the shear moduli and ν_{TT}, ν_{TL}, ν_{LT} are the Poisson's coefficients. By adding the symmetry of the compliance matrix and the transverse isotropy in Eq. (10), the number of independent variables is reduced to 5:

$$G_{TT} = \frac{E_T}{2 * (1 + \nu_{TT})} \tag{10}$$

The material inputs (cellulose content and crystallinity) were chosen in agreement with experimental values assessed on the same batch origin [50], i.e. a cellulose content of 75% and cellulose crystallinity of 60%. A homogenisation law materialised by two consecutive rules of mixtures was used to determine the elastic properties of the cell walls from their main constituents found in literature, following the procedure detailed in [58, 59]. The matrix was considered made of hemicellulose only, as the pectins and lignin content is low in the cell wall [7, 13]. Poisson's coefficient ν_{TT} was set to 0.2, knowing that its magnitude does not influence Young's modulus. Details of the resulting elastic constants can also be found in [58].

Since the MFA is considered in this study, the material is no longer considered as transverse isotropic in the local coordinate system (x,y,z). Therefore, the new stiffness tensor $[C^e]$ is expressed as a function of the MFA called φ in the local coordinate system by using the following equation:

$$[C^e] = [T] * [C^{*e}] * T^T \tag{11}$$

with [T] a rotation matrix dependant of φ:

$$[T] = \begin{bmatrix} 1 & 0 & 0 & 0 & 0 & 0 \\ 0 & \cos^2\phi & \sin^2\phi & 2\cos\phi\sin\phi & 0 & 0 \\ 0 & \sin^2\phi & \cos^2\phi & -2\cos\phi\sin\phi & 0 & 0 \\ 0 & -\cos\phi\sin\phi & \cos\phi\sin\phi & \cos^2\phi - \sin^2\phi & 0 & 0 \\ 0 & 0 & 0 & 0 & \cos\phi & -\sin\phi \\ 0 & 0 & 0 & 0 & \sin\phi & \cos\phi \end{bmatrix} \tag{12}$$

Finally, φ is evolving with the strain according to experimental data from SWING curve fitted equations in order to consider the evolution of MFA upon tensile testing. The load conditions are simulated through the displacement increase according to the experimental conditions and all computations are conducted using the COMSOL Multiphysics® software [60], with φ and consequently the stiffness matrix being modified at each displacement step following different evolutions developed below

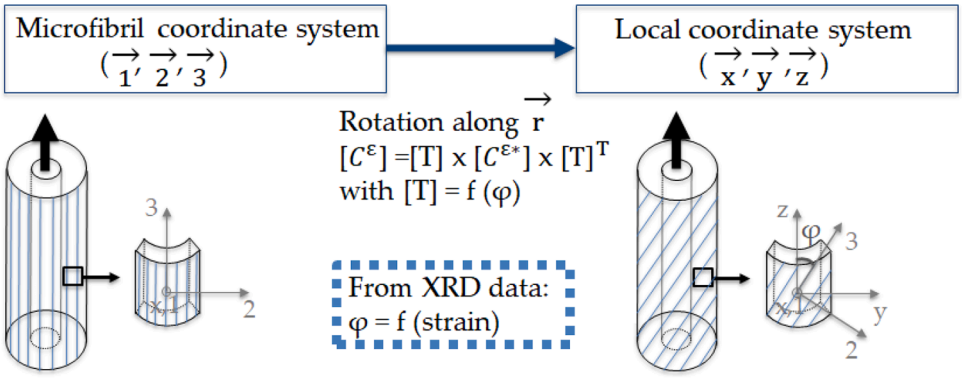

$$[C^{\varepsilon*}] = \begin{bmatrix} C_{11} & C_{12} & C_{13} & 0 & 0 & 0 \\ C_{12} & C_{22} & C_{23} & 0 & 0 & 0 \\ C_{13} & C_{23} & C_{33} & 0 & 0 & 0 \\ 0 & 0 & 0 & C_{44} & 0 & 0 \\ 0 & 0 & 0 & 0 & C_{55} & 0 \\ 0 & 0 & 0 & 0 & 0 & C_{66} \end{bmatrix} \quad [C^{\varepsilon}] = \begin{bmatrix} C_{11} & C_{12} & C_{13} & C_{14} & 0 & 0 \\ C_{12} & C_{22} & C_{23} & C_{24} & 0 & 0 \\ C_{13} & C_{23} & C_{33} & C_{34} & 0 & 0 \\ C_{14} & C_{24} & C_{34} & C_{44} & 0 & 0 \\ 0 & 0 & 0 & 0 & C_{55} & C_{56} \\ 0 & 0 & 0 & 0 & C_{56} & C_{66} \end{bmatrix}$$

Fig. 6. Principle of the FE model taking into account the MFA and related stiffness matrix.

for each model. The adjustments, involving the evolution from a transverse isotropic material expressed in the microfibril coordinate system to a material no longer transverse isotropic in the local coordinate system, are summarized in Fig. 6.

The following boundary conditions were applied to simulate tensile testing conditions: a displacement d was applied to the nodes of the lower surface in the direction 3 and the upper surface of the fibre was clamped (i.e. displacement at all nodes of the surface equal to 0 in all directions), summarized in the following equations, with U_1, U_2 and U_3 the displacements in the directions 1, 2 and 3 respectively:

$$\text{Upper surface}: \ U_1 = U_2 = U_3 = 0 \tag{13}$$

$$\text{Lowersurface}: \ U_1 = U_2 = 0; \ U_3 = d \tag{14}$$

The longitudinal Young's modulus E_{33} is calculated following Hooke's law as the ratio between the resulting stresses and strains. The engineering stress and strain values are determined using the Eqn 15 and 16, where F_3 is the reaction force in the direction 3, S is the surface of the filled fibre, d is the displacement imposed and L is the fibre length. In particular, the resulting stress is expressed from the mean between the surface integrals of the reaction forces at the nodes of both fibre edges since they do not have the same transverse surface areas.

$$\sigma = \frac{1}{2}\left(\frac{\iint F_{3\ (x=0)}}{S_{(x=0)}} + \frac{\iint F_{3\ (x=d)}}{S_{(x=d)}}\right) \tag{15}$$

$$\varepsilon\ (\%) = 100 * \frac{d}{L} \tag{16}$$

The relative difference of apparent modulus between two states is calculated as follow, with E_i the apparent modulus of the initial state and E_f the apparent modulus of the final state:

$$\%\ difference = 100 * \frac{E_i - E_f}{E_i} \tag{17}$$

The studies were performed under the hypothesis of a quasi-static analysis, using a direct solver. The calculations were performed thanks to a high-performance computer equipped with 1 TB of RAM and a bi-socket architecture operating at 4.4 GHz.

2.5.1. Influence of the MFA on Young's modulus

- Cylindrical fibres M0 and M10, with a porosity content of respectively 0 and 10% corresponding to the central lumen, an external diameter of 15 μm and a length of 140 μm were created and meshed directly using Comsol software.
- The MFA was varied between 0 and 60°.
- For each microfibril angle, the resulting Young's modulus was calculated at a displacement rate corresponding to 1% deformation, as only one loading step was required.

2.5.2. Evolution of Young's modulus upon microfibril realignment

- 3D volumes of fibres called **Fa, Fb, Fc**, and **Fd** obtained from X-ray microtomography were meshed using Simpleware™ ScanIP [61] and tetrahedrons of the second order (serendipity elements, quadratic discretization), with 3 degrees of freedom (dof) at each node corresponding to the displacements in the x, y and z directions. A mesh sensitivity analysis was performed in order to find the best compromise in terms of calculation time / accuracy of the result by varying the meshing coarseness of fibre **Fa** [50]. The optimal meshing coarseness was applied to all fibres, leading to numbers of dof between $0.5.10^6$ and 5.10^6. In order to compare the results and better quantify the consequences of the intricate lumen shapes evidenced by X-ray microtomography, cylindrical fibre models with a diameter of 15 μm, a length of 140 μm and a varied lumen content from 0 to 10% (M0 and M10 respectively) were created and meshed directly on Comsol software.
- A 4th order polynomial function is used to represent the kinetics of realignment of fibres $\boldsymbol{A_4}$ and $\boldsymbol{A_5}$ (SWING curve fitted equations of two contrasted fibres) are the following, with φ the MFA (°) and ε the engineering strain level (%):

$$\phi_{A_4} = 0.52 * \varepsilon^4 - 1.80 * \varepsilon^3 + 1.73 * \varepsilon^2 - 0.51 * \varepsilon + 5.23 \tag{18}$$

$$\phi_{A_5} = 1.94 * \varepsilon^4 - 7.53 * \varepsilon^3 + 9.22 * \varepsilon^2 - 4.33 * \varepsilon + 6.63 \tag{19}$$

- The model is no longer linear elastic due to the varied stiffness upon loading; therefore, parametric studies with displacements corresponding to deformations between 0% and 1.7%, with a step of 0.1%, were applied, in agreement with experimental data.

2.5.3. Heterogeneous microfibril orientations along the fibres

- A cylindrical fibre model M0 × 6 made of 6 cylinders with a diameter of 15 μm, a length of 200 μm and no central lumen was created and meshed directly using Comsol software.
- In a first part, the fibre M0 × 6 was modelled following the experimental results of setting 2 (Fig. 3, fibre $\mathbf{B}_1$) over 1 mm (between $x = -3$ and $x = -2$ mm) to keep a reasonable calculation time. The MFA evolutions for the 6 consecutive cylinders were the following, with φ the MFA (°) and ε the strain (%):

$$\phi = \begin{pmatrix} \phi_1 \\ \phi_2 \\ \phi_3 \\ \phi_4 \\ \phi_5 \\ \phi_6 \end{pmatrix} = \begin{pmatrix} 5.81 \\ 0.51 * \varepsilon^2 - 1.06 * \varepsilon + 5.52 \\ 5.37 \\ 0.28 * \varepsilon^2 - 0.96 * \varepsilon + 7.07 \\ 6.29 \\ 0.78 * \varepsilon^2 - 1.79 * \varepsilon + 7.46 \end{pmatrix} \tag{20}$$

In a second study, two different MFA evolutions were implemented for the fibre M0×6: the MFA was set constant at 5° to represent non-defected areas, and an initial MFA of 30° decreasing linearly to 5° at 1.3% strain was set to represent defects. The number of cylinders imbedding defects was varied between 0 and 6, corresponding to a defect quantity ranging from 0 to 100%. As only Young's modulus was investigated here, when considering the same number of cylinders representing defects, the results were not influenced by their position along the fibre.

- For fibre M0×6, parametric studies with displacements corresponding to deformations between 0% and 1.3% were applied, in agreement with experimental data.

3. Results and discussion

3.1. Experimental evidence

3.1.1. Reference tensile testing

The reference tensile tests without X-ray diffraction evidenced a mean Young's modulus of **39.3 ± 12.3 GPa**, strain at break of **2.24 ± 0.83**% and strength at break of **700 ± 268 MPa (Table 2)**. The tensile values appear in the average in terms of strain at break and in the lower bound in terms of Young's modulus and strength at break compared to literature data [62].

3.1.2. Realignment of cellulose microfibrils under continuous tensile testing

In situ tensile tests were conducted on 9 unitary fibres with contrasted defect content expressed in Table 4, following the setting 1 (Fig. 3, continuous tensile testing, horizontal fibre). The resulting MFA

Table 2
Summary of different fibre geometries and related parameters used for the finite element analysis. The fibre geometries which include variations of cross-sectional areas along their length are specified in the fifth column.

Name	Porosity content (%)	Degrees of freedom (Dof) ($x10^6$)	Mean volume of element ($x10^{-3}$ μm^3)	Variations along fibre length	Modelling configuration (Fig. 5)
Fa	7.30	2.2	15	X	2
Fb	2.60	4.3	15	X	2
Fc	0.01	4.8	25	X	2
Fd	0	4.2	23	X	2
M0	0	0.5	207		1 – 2
M10	10	0.7	135		1 – 2
M0 × 6	0	0.6	166		3

evolutions as a function of strain are plotted in Fig. 7, revealing contrasted behaviours. Indeed, MFA initial values vary between 4.7° and 7.4° depending on the fibre (Table 4), in agreement with previously reported XRD measurements (Table 1). Other techniques such as second-harmonic generation microscopy under controlled polarised light also revealed MFA inhomogeneities along flax fibres [10], with values varying between 0° and 10° and an average around 5°. Moreover, a microfibril realignment ranging between 3 and 24% upon tensile testing was observed depending of the sample. Therefore, rearrangement of cellulose microfibrils in the cell walls seem to appear in most cases upon tensile testing, as already reported in the literature [18, 30, 31, 63]. Moreover, one must keep in mind the high strain rate of 6.7%/min used in this study following the 1 mm / min displacement rate specified in NF-T 501–2 standard, which can explain the limited reorientation of microfibrils compared to other studies in the literature conducted with a lower strain rate, due to the viscoelastic nature of flax. The low mechanical properties obtained in XRD-coupled tests compared to the mean values obtained under laboratory conditions (without X-ray beam) can partly be attributed to damage induced by irradiation. Indeed, while the mean strain at break of 1.61 ± 0.52% appears 30% lower for the XRD-coupled tests in comparison to reference tests, a decrease of more than 50% is observed for the mean strength of 318 ± 82 MPa (Table 2). However, no significant differences between the samples scanned with different X-ray beam size in length and resulting acquisition times were evidenced. We should also keep in mind that the gauge length of the reference tensile test is 10 mm, whereas it is 15 mm for in situ tensile tests due to technical specifications of the machine. The strength might be lowered for the higher gauge length following the weakest link theory developed by Griffith [64].

The discrepancies encountered in this study in terms of microfibril initial values and evolution upon tensile testing might partly explain the complex mechanical response of plant fibres. Indeed, most plant fibres including flax present a predominant non-linear response to tensile loading [65]. Numerous authors tried to decipher the underlying mechanisms, which remains a moot point due to difficult experimental validation. Among the possible influential factors, one can mention the biochemical composition [65], fibre shape and internal lumen [40, 59], ultrastructural parameters including the microfibril orientation [39] especially in defects [45, 66], and strain-induced crystallisation of paracrystalline cellulose [30]. Unfortunately, the non-linearities of the stress-strain curves were not accessible during our experiment due to the insufficient resolution of the load cell in the tensile experiment. The disparities observed in our study may find their origin in experimental parameters or intrinsic variabilities of the fibres detailed below.

a **Experimental parameters:**

Although great efforts have been made in the last decades to standardize mechanical characterization of plant fibres, experimental variabilities remain inherent to the characterization of small entities such as flax fibres. In our study, the fibres ***A3, A8*** and ***A9*** exhibit a phase of MFA increase followed by a decrease, when increasing strain, which is attributed to the presence of a twist in the fibres before tensile testing, revealed by optical microscopy. Indeed, the presence of a twist might result locally in a higher microfibril angle, as shown by Burgert et al. [67], who observed a MFA increase from 5 to 12° between untwisted and twisted individual chemically isolated wood fibres by WAXS measurements. During tensile testing, as the fibre is stretched it may unfold in order for its mass centre to reach back equilibrium on the median line. Therefore, the twist might reach gradually the X-ray measurement location before disappearing upon stretching. This phenomenon of MFA increase followed by a decrease was not observed on experiments performed at the fibre bundle scale, where the fibre torsion is likely to be prevented by the neighbouring cells. The experiments at the fibre bundle scale are not presented in detail here as it is not the scope of the present article. These local twists highlight the experimental difficulties induced by the handling of such small entities, but also the need to consider the possible rotation induced by specific environmental relative humidity conditions. Indeed, anti-clockwise rotation of the fibres upon drying was witnessed by several authors [67–69]. For instance, Placet et al. [26] observed a lower yield point and an additional increase in stiffness for a twisted fibre compared to its second half with no rotation, revealing a modification of cell wall. In addition, the low defect content, inducing a small initial MFA and strains at break of fibres ***A1*** and ***A3*** (4.7 and 4.8° respectively with strains at break of 0.8 and 1%) might be attributed to

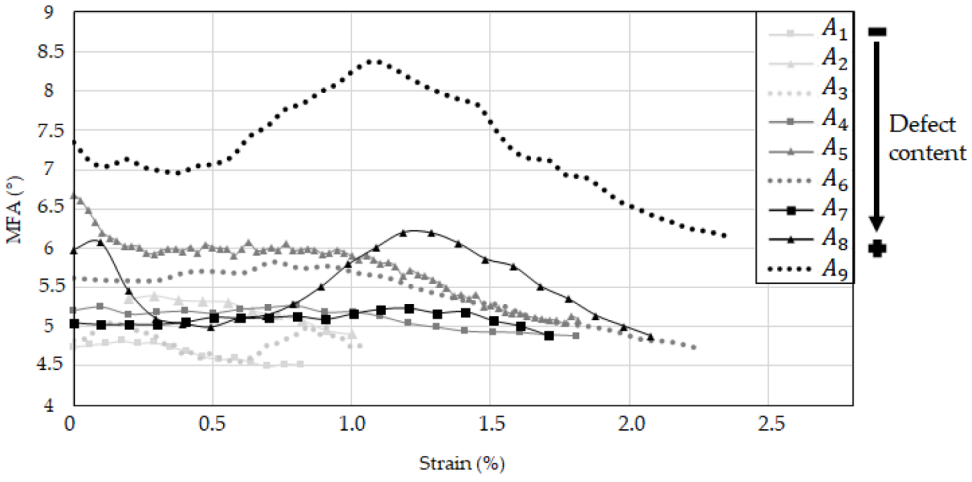

Fig. 7. Microfibril angle of different unitary fibres calculated during a tensile test, as a function of strain.

an initial pre-tension applied by the operator upon sample preparation. In the same vein, as the XRD acquisition started at a strain of 0.2% for fibre A_2, the behaviour at the onset of stretching is lacking, likely inducing an underestimation of the initial MFA and overall realignment. Furthermore, misalignment of a fibre arguably may contribute to discrepancies in the results because in the tensile machine, it might induce additional shear, which might in turn influence the ability of the microfibrils to realign in the surrounding matrix. The misalignment can arise either from the positioning of the fibre on the cardboard or from the positioning of the cardboard on the tensile device. Finally, as discussed in part 2.4., the calculation method induces uncertainties depending on the fibre shape [19], which might contribute to the differences observed from one fibre to another.

b **Intrinsic variabilities:**

Quantification of defects and reversible disappearance upon tensile testing were observed by several authors upon tensile testing thanks to polarized light microscopy [26, 66]. Moreover, some authors evidenced microfibril reorientation in a flax fibre with heterogeneous initial orientation [31]. However, up to our knowledge the direct link between defects and microfibril angle changes upon tensile testing was never assessed before. In our study conducted on contrasted fibres in terms of defect quantities, a correlation between the defect quantity and initial/final MFA is evidenced in Fig. 8a, with linear determination coefficients of 0.7. The initial MFA values corroborate with the microfibril misalignment observed by several authors in defects [17, 70]. Moreover, the trend towards a more important realignment for unitary fibres with higher initial MFA is evidenced in Fig. 8b.The defect density might partly explain the differences observed in terms of initial MFA and realignment, and therefore mechanical properties. Moreover, a trend towards a higher realignment in the last part of the tensile testing is observed in Fig. 7, in agreement with the qualitative observations of defect disappearance described by Placet et al. [26], attributing the stiffening occurring in last part of the stress-strain curves to the realignment of cellulose microfibrils, especially in defects. In addition, the cross-sectional variations inherent to plant fibres [3] might induce additional shear stresses in some fibres, again influencing the stick-slip mechanism, interfaces and ease of the microfibrils to realign upon tensile testing. Moreover, rotation of the fibre can also appear upon tensile testing for the thinnest-walled fibres, as a result of buckling induced by shear strains [71, 72]. Finally, the matrix properties and composition themselves may differ from a fibre to another and again influence the microfibril ease of movements.

Two fibres contrasted in terms of defect quantity and realignment behaviour (fibre A_4 and A_5) were selected as inputs for the FE model. Their MFA, stress evolution as a function of strain, and related defect density evidenced by polarized light microscopy are plotted in Fig. 9. Fibre A_5represents a higher defect density (22% of the total fibre area), an initial MFA of 6.7° and important realignment of 24.1%, whereas fibre A_4 exhibits less defects (8% of the total fibre area), a lower initial MFA of 5.2° and realignment of 6% upon tensile testing (Table 4). Interestingly, a MFA realignment with three different slopes is evidenced for fibre A_5(Fig. 9), which resemble to the stress-strain curves non-linearities in three phases encountered with most plant fibres [65]. The mechanical properties of fibres A_4 and $A_5$are similar with a strain at break of 1.73% and a strength of 340 and 308 MPa respectively, despite their different MFA values and evolution. It highlights the difficulty to correlate local information such as MFA measurements at one particular location along the fibre with global mechanical properties. Therefore, XRD measurements were taken at different locations along the fibres in the next part of the study to better characterize the fibre globally.

3.1.3. *Heterogeneous microfibril orientation along fibres*

The MFA evolution along unitary fibres with contrasted defect densities was revealed by X-ray diffraction mappings and stepwise tensile testing using X-ray beam lengths of respectively 250 and 20 μm (settings 2 and 3 in Fig. 3). With setting 2, heterogeneous microfibril orientations along fibre B_1 are revealed at different strain steps comprised between 0 and 1.3% corresponding to stresses up to 110 MPa (**Fig. 10**). Indeed, while most of the fibre exhibits MFA between 5 and 8°, the area close to the right extremity shows a MFA reaching 17° at 0.2% strain, in agreement with the bright area observed under polarized light, characteristic of the presence of numerous defects. At this location, the MFA at 0% strain could not be calculated because the fibre was not entirely straight and the area dropped out of the X-ray beam. Despite the experimental issue, the fibre represents a realignment ratio of more than 50% between 0.2 and 1.3% strain. Within the rest of the fibre, realignment fluctuates between −7 and 25%. The negative values appear within the error range of 0.5° (Fig. 4). It is assumed that no microfibril rearrangement at these locations occur. The tendency observed towards a preferential realignment in the most misaligned microfibrils is confirmed by the findings of Kölln et al. [31] and agrees with the results of continuous tensile testing displayed in Fig. 8b. Although the link between high MFA and defects observed under polarized light is clear for the extreme right of the fibre, it is less obvious for the left part. Indeed, experimental limits are arguably the output as the error of spatial correlation between optical image and X-ray location is

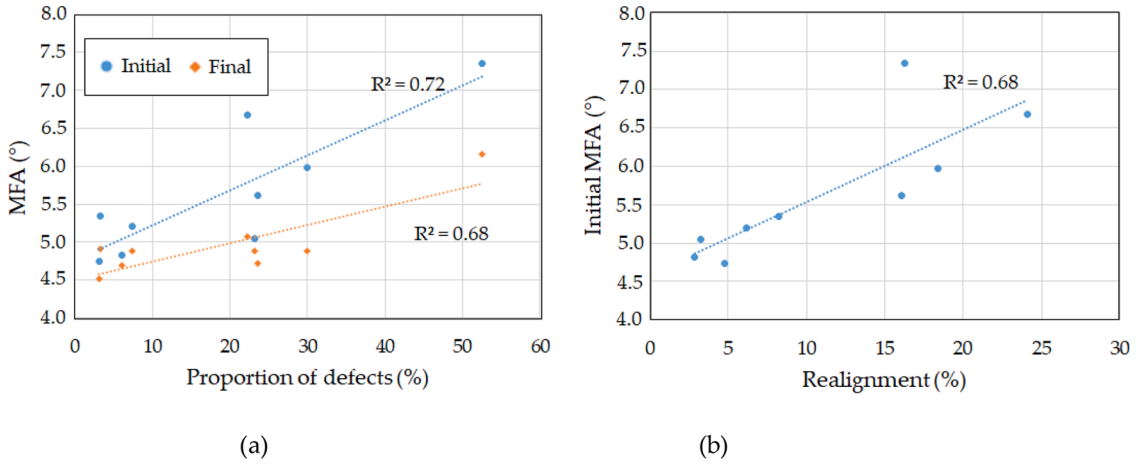

Fig. 8. (a) MFA of different unitary fibres measured at the initial and final steps of tensile testing, as a function of the proportion of defects; (b) MFA of different unitary fibres calculated at the first step of tensile testing, as a function of the final realignment. The values of R^2 represent the linear determination coefficients associated to the curves.

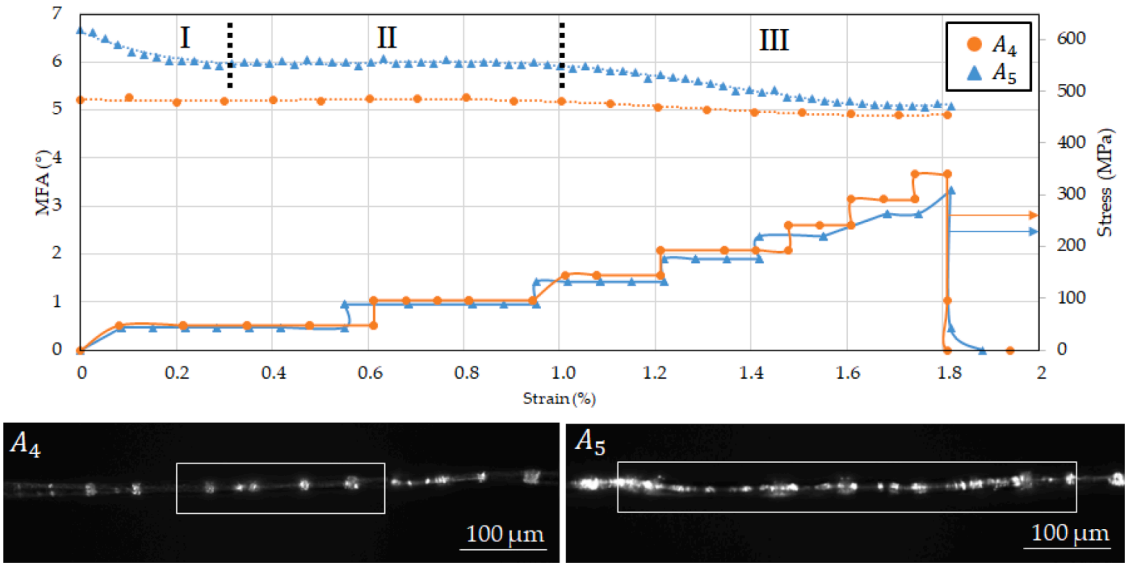

Fig. 9. Top: MFA and stress evolutions as a function of strain for two fibres A_4 and A_5, with contrasted defect density observed by polarized light microscopy (bottom). The X-ray beam, of 250 and 550 µm in length for fibres A_4 and A_5 respectively, was positioned at the centre of the initial microscopy image and is represented as a white rectangle above. The dotted lines delimit the three parts of the non-linear MFA evolution of A_4 (I, II and III).

Table 3
Results of reference tensile testing and *in situ* tensile testing (mean values of Table 4).

	Young's modulus (GPa)	Strength at break (MPa)	Strain at break (%)
Reference tensile testing	39.3 ± 12.3	700 ± 268	2.24 ± 0.83
In situ tensile testing	–	318 ± 82	1.61 ± 0.52

estimated to 100 µm and X-ray measurements are averaged on 250 µm in this configuration. This lack of spatial resolution might explain the lower values obtained in defects compared to literature [17, 70]. Indeed, Thygesen et al. [70] reported MFA of up to 30° in large dislocations surrounded by zones of intermediate orientations with MFA between 10 and 15° in hemp fibres using polarized Raman microspectroscopy. The work of Melelli et al. [17] is in agreement with such results, as authors measured strongly heterogeneous macrofibril orientations ranging from 0 to 47° in flax fibres by SHG imaging under controlled polarised light.

To increase the X-ray spatial resolution, the setting 3, with a X-ray beam of 250 × 20 µm and the fibre placed vertically (Fig. 3) was used,

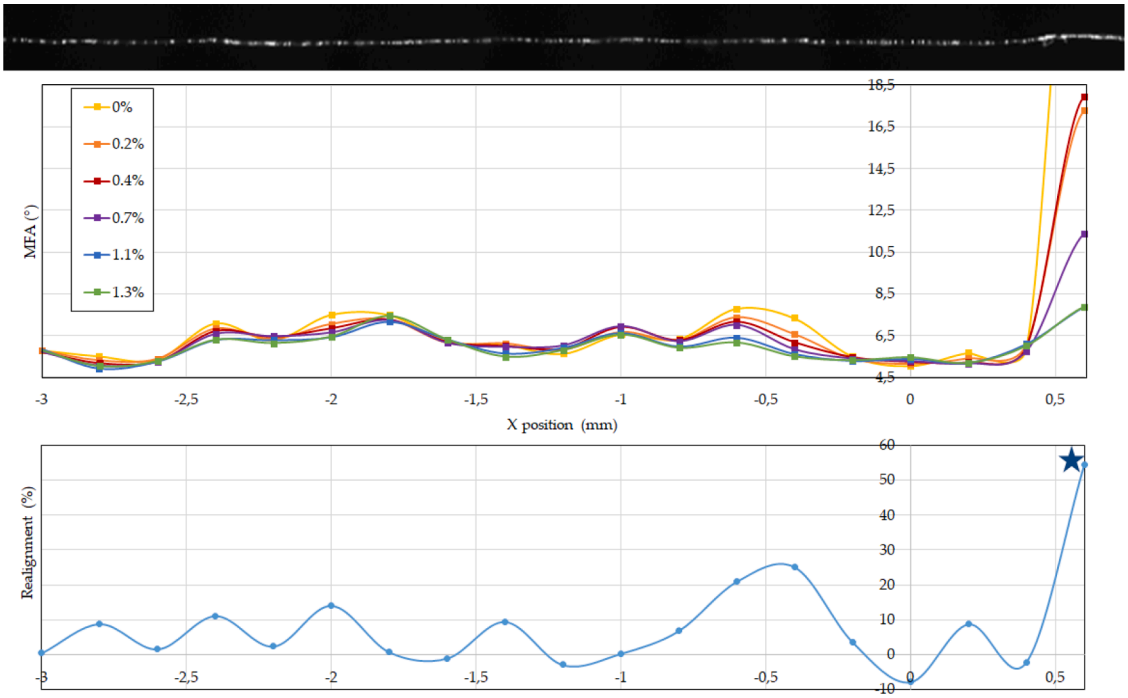

Fig. 10. View of fibre B_1 under polarized light revealing defects as bright areas (top); MFA measurements along the fibre at different strains (from 0 to 1.3%) using setting 2 (middle); and corresponding realignment (bottom) calculated between the first and last tensile steps (except for the star marked value which is an estimation between the second and last step of tensile testing).

leading to the MFA evolution along fibre $\mathbf{B_2}$ displayed in Fig. 11. X-ray measurements were taken every 50 μm along the z-direction at 0% and 0.4% strain, corresponding to stress levels of 60 and 166 MPa, representing low stress level as a mean tensile strength of 700 ± 268 MPa was reported for the reference tensile testing on the same variety and growth conditions. To explain the early failure at 0.4% strain, the hypothesis of a possible damage induced by repeated and long (4 s) X-ray irradiation is put forward. The MFA varies between 4.5 and 7.7°, with significant realignment superior to 5% observed in the central part of the fibre (between −3 and −2.5 mm) and around −4 mm, which correspond to defected areas according to the corresponding polarized light view.

3.2. Numerical predictions

3.2.1. Influence of the MFA on fibre overall stiffness

The influence of the MFA on Young's modulus is considered through a finite element model that is applied to the cylindrical fibre models M0 and M10 (with a porosity content of respectively 0 and 10%). This computation aims at investigating the link between the microfibril angle and resulting Young's modulus. As evidenced in Fig. 12, Young's modulus decreases non-linearly as the microfibril angle increases, with a steeper trend for low MFA, reaching more than 30% of drop in stiffness between a MFA of 0° and a MFA of 10°. Moreover, the decrease reaches a plateau after 40°. Regarding the influence of porosity, the relative difference in apparent modulus between M0 and M10 is constant with a value of 10% regardless of the MFA, explained by a rule of mixture between the cell wall material and air. The decrease of Young's modulus upon MFA increase observed in Fig. 12 is in agreement with analytical and FE models developed by several authors [27, 38, 39, 42, 43, 46]. With MFA values determined experimentally (red dotted lines, from Table 1), the resulting Young's modulus varies between 40 and 60 GPa, in agreement with experimental data [62]. The major effect of the cellulose MFA on Young's modulus is explained by the high stiffness of crystalline cellulose ($E = 134$ GPa) compared to the surrounding matrix constituents [38]. Therefore, the microfibril orientation, cellulose content and crystallinity strongly influence the overall fibre Young's modulus. Therefore, the low MFA combined to a high cellulose content and crystallinity reported for hemp and flax fibres partly explain their higher tensile properties compared to cotton or wood fibres for instance.

3.2.2. Evolution of Young's modulus upon microfibril realignment

The consequences of the different MFA evolutions on the longitudinal Young's modulus were investigated thanks to the fibre model involving contrasted porosity content (M0 and M10) and on fibre geometries **Fa, Fb, Fc** and **Fd** obtained by X-ray microtomography. The resulting apparent moduli are plotted as a function of strain in Fig. 13 considering the MFA evolution obtained experimentally for fibres $\boldsymbol{A_4}$ and $\boldsymbol{A_5}$ respectively (Fig. 9), with curve fitting using polynomials of the 4th order. Compared to the model with MFA = 0°, a decrease in initial modulus of 11 and 17% is observed with the initial MFA of fibres $\boldsymbol{A_4}$ and $\boldsymbol{A_5}$respectively**.** The phenomenon is observed for all fibre geometries but visible here for the cylindrical model fibres, when comparing the initial moduli values of the curves M0 and M10 in Fig. 12 and the initial moduli values of the curves M0 and M10 in Fig. 13. Upon decreasing MFA, a fibre stiffening effect is confirmed by the numerical model in both cases, reaching 1.5% and more than 7.5% following the MFA evolution of $\boldsymbol{A_4}$ and $\boldsymbol{A_5}$ respectively. This observation agrees with the numerical results of several authors. Indeed, a micromechanical model derived by Baley [27] concluded to a Young's modulus which almost doubled upon tensile testing. However, the rather strong hypothesis of complete microfibril realignment (ranging from 10 to 0° upon tensile testing) was currently not confirmed by any experimental results. An important microfibril realignment (from 11° to 5.7° at 4% strain) was assumed in an elastic model conducted on hemp unitary fibres by Trivaudey et al. [44]. It resulted in a fibre stiffening with Young's modulus multiplied by 1.6, from 40 to 64 GPa. In our case, the lower stiffening

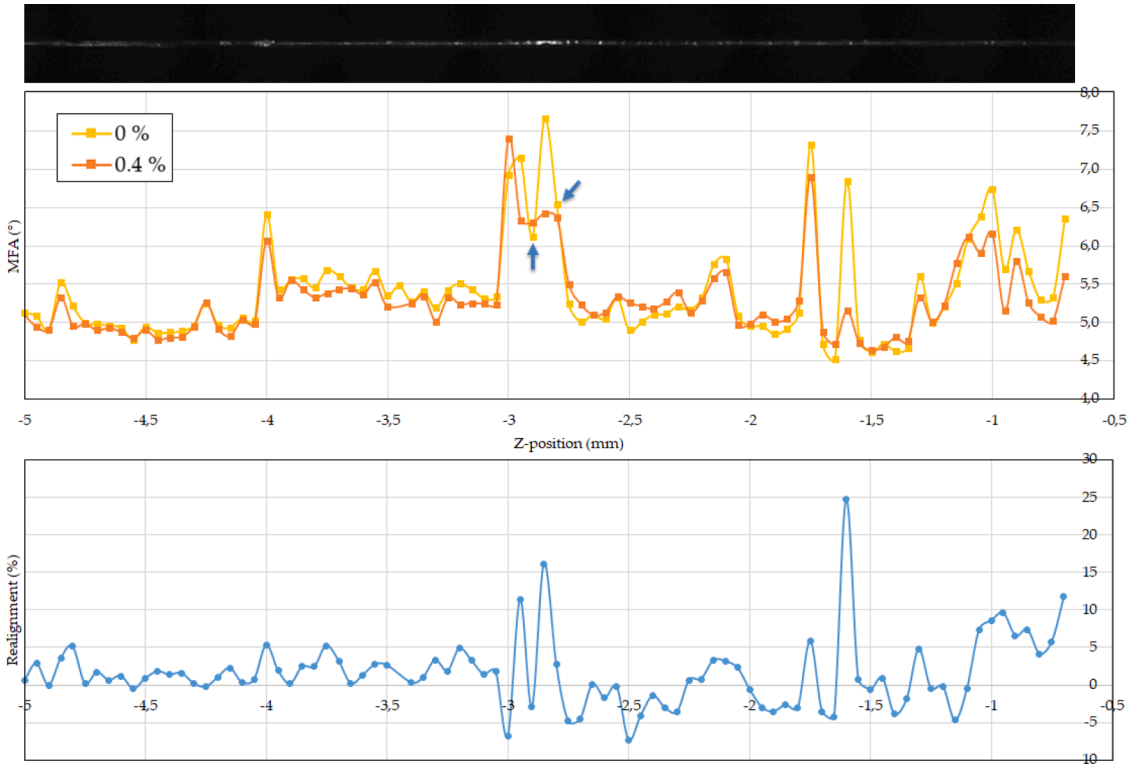

Fig. 11. View of fibre B_2 under polarized light revealing defects as bright areas (top); MFA measurements along the fibre at different strains (from 0 to 0.4%) using setting 3 (middle); and corresponding realignment calculated between the first and last tensile steps (bottom). The arrows point out values where a misalignment of the fibre thanks to the vertical axis might induce error in the resulting MFA.

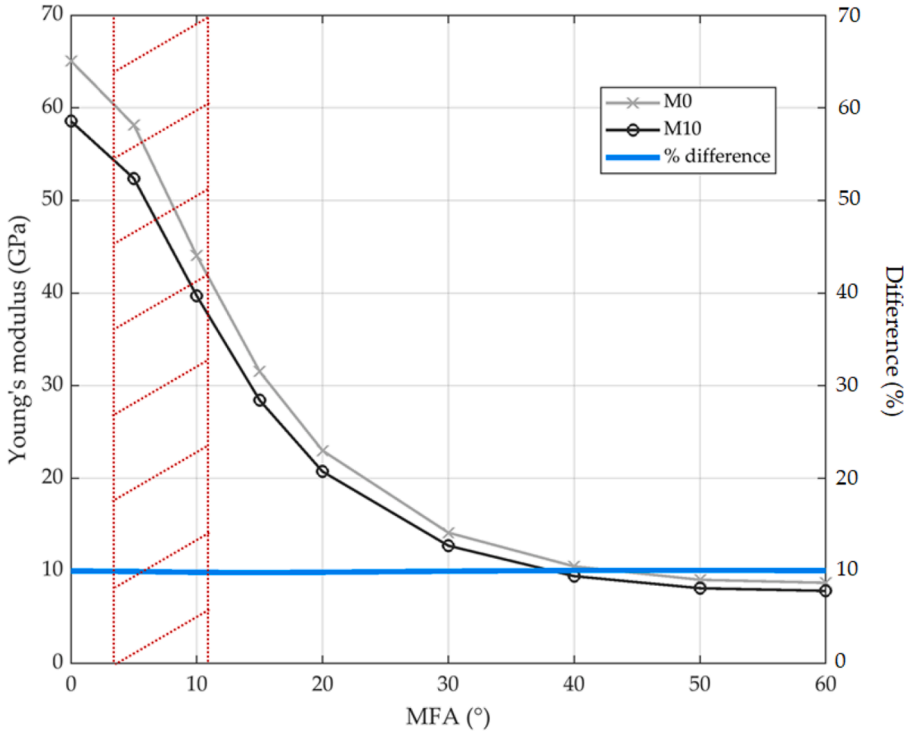

Fig. 12. Predicted Young's modulus E_{33} as a function of the microfibril angle resulting from the FE analysis performed on a filled cylindrical model fibre (M0) and with 10% porosity (M10). The difference in resulting modulus is also plotted as a percentage, and the values of MFA reported for dry flax in literature (Table 1) are displayed between the red dotted lines.

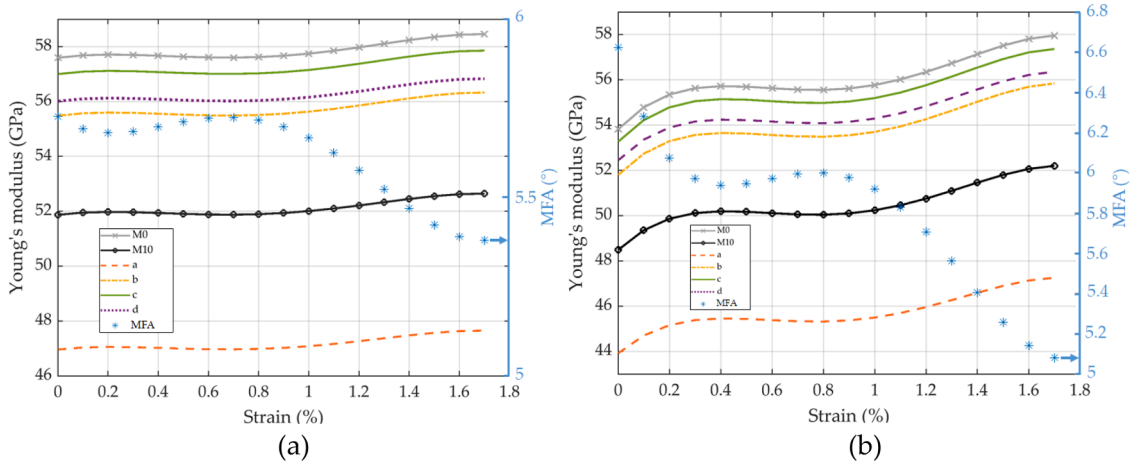

Fig. 13. Evolution of Young's modulus (left axis) for all considered fibres (Fa, Fb, Fc and Fd) and cylindrical model fibres with 0 and 10% porosity (M0 and M10), following the MFA evolution of fibre (a) A_4 and (b) A_5, as a function of strain.

can be explained by the lower MFA decrease implemented, in agreement with experimental data. Interestingly, the differences between Young's moduli of $\mathbf{A_4}$ and $\mathbf{A_5}$ decrease upon tensile loading to reach a similar value as a result of the more important realignment of fibre $\mathbf{A_5}$, ranging from around 47 – 58 GPa depending on the fibre geometry. Consequently, the final modulus is only 10 and 11% lower considering the MFA evolution of A_4 and A_5 respectively compared to the model with MFA = 0° at the end of the stress-strain curve (1.7% strain). The phenomenon is observed for all fibre geometries but visible here for the cylindrical model fibres, when comparing the initial moduli values of the curves M0 and M10 in Fig. 12 and the final moduli values of the curves M0 and M10 in Fig. 13. Therefore, in this case defected areas seem to reach a similar MFA than non-defected areas, and thus a similar stiffness after a more important stiffening.

The apparent modulus evolutions are similar for all fibre geometries. Therefore, no influence of the fibre morphology is visible here, contrary to some models developed in literature. Indeed, Del Masto et al. [40] have shown an influence of the degree of anisotropy on the non-linearities, greatly enhanced by taking into account the viscoelasticity of the material, which is not the case in our model. In addition, Gassan et al. [39] observed an increase of Young's modulus upon increasing degree of anisotropy, but the influence was only significant for highly elliptical fibres, i.e. with a ratio lower than 0.4 between the largest and smallest half axes of the ellipse. Moreover, the differences of stiffness between the fibres were explained in another work developed by the team as a result of different porosity content and shearing induced by geometrical considerations [58]. The influence of the dimensional variations along fibres on their tensile behaviours was also developed in

a numerical model by He et al. [73, 74].

The predicted stress-strain curves for the extreme geometry cases (fibres **M0** and **Fa**) following the MFA evolution of fibres $\boldsymbol{A_4}$ and $\boldsymbol{A_5}$ and a constant MFA equal to 0° are plotted in Fig. 14, together with the experimental curves obtained for the reference tensile tested samples without X-ray irradiation. The numerical responses are closer to the experimental ones, with a lower apparent modulus, by taking into account a MFA greater than 5° (M0-A5, Fa-A5, M0-A4 and Fa-A5) compared to the curves obtained with a MFA equal to 0° (M0-MFA0 and Fa-MFA0). However, the differences of MFA evolution between fibres $\boldsymbol{A_4}$ and $\boldsymbol{A_5}$ are not sufficient to explain the variabilities encountered experimentally. Indeed, the stress-strain curve of the extreme cases of fibre geometries (**M0** and **Fa)** appear very close with both the MFA evolutions from $\boldsymbol{A_4}$ and $\boldsymbol{A_5}$. In addition, the curves obtained do not reflect the strong non-linearities observed for most fibres during tensile testing. Therefore, additional phenomena such as the plasticity of the matrix as well as viscoelasticity and possible shear-induced crystallisation of the cellulose should be considered both experimentally and numerically. Indeed, the viscoelasticity introduced in a FE model by Trivaudey et al. [44] leads to an initial stiffness decrease corresponding well to the beginning of the non-linear experimental stress-strain curves mainly observed for plant fibres. Moreover, the viscoelasticity that was implemented in this model also induced a higher MFA decrease upon tensile testing, which in turn contributed to an additional stiffening at the end of the stress-strain curve, in agreement with experimental data. Therefore, it could reflect the effect of water leading to a plasticization of the matrix and consequently an ease of realignment for the cellulose microfibrils. Moreover, the shear-induced crystallization introduced an additional stiffening which fitted well with experimental data but remains to be proven experimentally [31, 47]. The plasticity of the hemicelluloses caused a non-linearity closer to experimental behaviour in the work conducted by Nilsson et al. [45]. Finally, the interfacial phenomena induced by the presence of defects for instance, might be underestimated in this model. Therefore, a FE model taking into account the MFA heterogeneities encountered along fibres is developed in the next section, with the aim of better reflecting the global tensile response by relying on less localized experimental information.

3.2.3. *Heterogeneous microfibril orientations along the fibres*

According to SWING experimental results of setting 2 (Fig. 10), a slight increase of 4.3% in Young's modulus is revealed (Fig. 15a-SWING curve) as a result of the MFA decrease in the zones of higher initial MFA (Fig. 10). However, the non-linearity in the stress-strain curve is only minor and do not reflect the experimental non-linearities observed (Fig. 15b). As the experimental values might be under-estimated due to the experimental condition (X-ray beam length of 250 μm), more important initial MFA of 30° were tested to model defects in a second model. A linear realignment up to the level of adjacent free-of-defect areas (5°) was assumed and the initial value of 30° was chosen in agreement with experimental data reported by more localized techniques such as SHG microscopy or polarized Raman spectroscopy [17, 70]. The results show that the increase of defect content leads to a more important increase in Young's modulus upon tensile testing, with a stiffness increase ranging from 0 to more than 300% depending of the defect content (between the first and last modulus values in Fig. 15a). Moreover, the non-linearities are enhanced by the increasing defect content. Therefore, the defect quantity might partly explain the non-linearities and the variability observed experimentally, as defect quantities between 3% and 53% were reported in the experimental part of this study (Table 4). Trivaudey et al. [44] developed a fibre model with a defect density of 25% and a more important microfibril realignment in defected areas (from 30 down to 16° at 4% strain) than the neighbouring areas (from 11 to 3.5° at 4% strain). Considering viscoelasticity and strain-induced crystallization, they observed a significant decrease in apparent stiffness compared to the model without defect, which fitted well with experimental data. Moreover, the stress concentrations were enhanced using an elastic law compared to a viscoelastic one. Nilsson et al. [45] modelled dislocations with a ratio of 13% of the cell wall, and observed enhanced non-linearities as well. They used the assumption of a dislocation angle depending on the radius, which remains to be verified experimentally and could explain the diameter dependency of Young's modulus. However, in our case the hypothesis of an initial MFA of 30° in defected areas and realignment up to 5° is rather strong, and a stringent quantification using an X-ray microbeam upon tensile testing would help confirm the results.

4. Conclusions

This study investigated the cellulose microfibril realignment upon tensile testing depending on the defect density and heterogeneous MFA distribution along a fibre, as well as their consequences on the mechanical properties by combined experimental and numerical approaches.

The synchrotron X-ray diffraction results highlighted contrasted initial microfibril angles between 4.7 and 7.4° depending on the fibre. The realignment of microfibril towards the fibre direction upon continuous tensile testing was measured between 3 and 24% depending on the fibre. Defect density measurements by polarized light microscopy

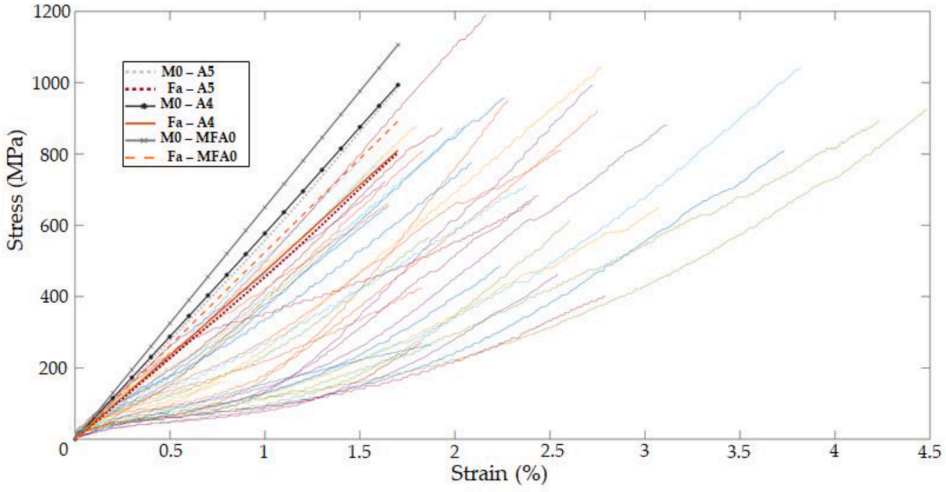

Fig. 14. Superposition of the reference stress-strain curves obtained experimentally on samples from the same origin without X-ray irradiation and the extreme numerical results (fibre geometries M0 and Fa) following the experimental evolution of MFA from fibres A_4 and A_5 and with a MFA = 0° (MFA0).

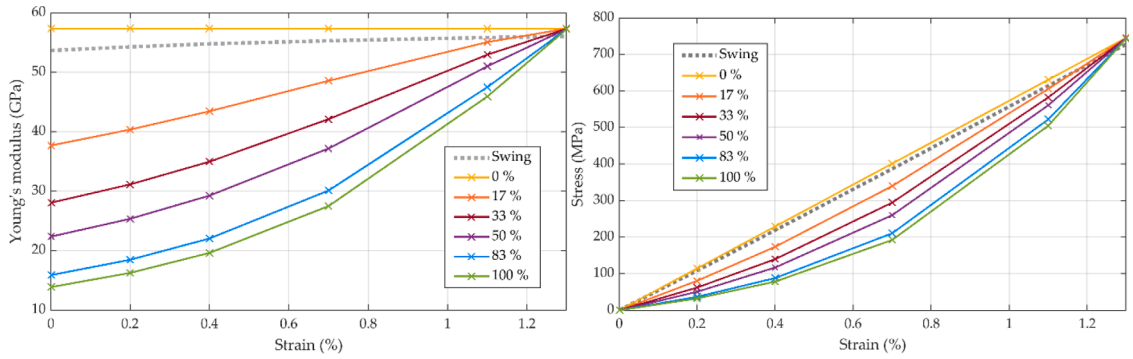

Fig. 15. Evolution of (a) Young's modulus and (b) the axial stress as a function of strain for fibres M0 × 6 following 1) SWING experimental results of setting 2 (Swing) and 2) 6 fibres with increasing defect content from 0 to 100%, expressed in%, with a MFA set constant at 5° to represent non-defected areas, and an initial MFA of 30° decreasing linearly to 5° at 1.3% strain was set to represent defects.

Table 4
Evolution of the MFA, defect quantities and mechanical properties obtained from continuous tensile testing for unitary fibres with different defect density. The fibres A_4 and A_5 (in bold) were chosen as inputs for the finite element analysis.

Sample	X-ray beam size (μm)	Initial MFA (°)	Realignment (%)	Defect quantity (%)	Strength (MPa)	Strain at break (%)
A_1	550	4.7	4.8	3.1	407	0.80
A_2	250	5.4	8.2	3.3	386	1.0
A_3	550	4.8	2.9	6.0	239	1.0
A_4	**250**	**5.2**	**6.2**	**7.5**	**340**	**1.73**
A_5	**550**	**6.7**	**24.1**	**22.3**	**308**	**1.73**
A_6	250	5.1	3.3	23.2	214	1.73
A_7	250	5.6	16.0	23.6	455	2.20
A_8	250	6.0	18.4	29.9	298	2.0
A_9	550	7.4	16.3	52.5	212	2.33

enabled to underline the trend towards a higher MFA for the most defected fibres, leading to a more important realignment upon tensile testing, with linear determination coefficients of 0.7. Variations of cross-sections along fibres and matrix properties are as intrinsic parameters involved in the variability of MFA evolutions upon tensile testing. In addition, the influence of experimental parameters such as the possible pretension, twisting and misalignment of the fibres was pointed out. Finally, the heterogeneous MFA along flax fibres and reorientation were evidenced by stepwise tensile testing with an X-ray beam length reaching 20 μm with MFA initial values reported between 4.5 and more than 17°. The realignment upon tensile testing varied between 0 and more than 50% along the fibres. Moreover, a more homogeneous MFA distribution was reached upon tensile testing, as zones of higher initial MFA presented the highest values of realignment. However, the experimental resolution achieved was not sufficient to depict transition zones and single defects in the range of the μm in size. As a prospect, next experiments will overcome the experimental issues described, with the use of a goniometer to better control and assess the alignment and twist of the fibre, as well as an X-ray microbeam to reach a higher spatial resolution, ideally close to the μm. In terms of data analysis, it would also be of interest to investigate the possible strain-induced crystallisation of cellulose and the cellulose crystallites elongation in the fibre direction, by recording the diffraction spot corresponding to the planes (004). Observation of fracture surfaces will also help deciphering the influence of defects on the failure mechanisms.

The results of finite element modelling show the major influence of the cellulose microfibrils on the tensile response, with a non-linear decrease of the overall Young's modulus upon increasing microfibril angle, from values between 58 and 65 GPa at MFA = 0°, depending linearly of the porosity content, up to a threshold around 10 GPa above 40°. Following the contrasted MFA realignment upon tensile testing obtained experimentally for two fibres, a stiffening between 1.5 and 7.5% was observed as a result of the finite element model depending on the MFA evolution law, reaching a similar value. No influence of the fibre aspect ratio on Young's modulus was reported, probably because of the simplicity of the elastic model. Moreover, the results only partly explained the non-linearities observed experimentally. The last model took into account the heterogeneous MFA distribution by implementing different laws of MFA evolution along the fibre. Based on the experimental values, a limited stiffness increase of 4.3% was observed. Assuming defects as zones of initial MFA of 30°, in line with experimental data obtained with spatially resolved SHG microscopy, and linear decrease up to 5°, the values of non-defected areas, enhanced nonlinearities were observed upon increasing defect content. As a prospect, the next models should take into the viscoelasticity and plasticity of the matrix, as well as more spatially resolved description of the MFA. Finally, it would be of interest to investigate stress concentrations in view of deciphering the failure mechanisms.

Funding

This research was funded by the INTERREG VA FCE Program, FLOWER project, Grant Number 23.

Conflicts of interest

The authors declare no conflict of interest. The funders had no role in the design of the study; in the collection, analyses, or interpretation of data; in the writing of the manuscript, or in the decision to publish the results.

CRediT authorship contribution statement

E. Richely: Conceptualization, Validation, Formal analysis, Investigation, Writing – original draft, Writing – review & editing, Writing – review & editing, Visualization. **L. Nuez:** Investigation, Writing – review & editing. **J. Pérez:** Formal analysis, Investigation, Resources, Writing – review & editing. **C. Rivard:** Investigation, Writing – review & editing, Writing – review & editing. **C. Baley:** Validation, Writing – review & editing, Supervision. **A. Bourmaud:** Validation, Investigation, Writing – review & editing, Supervision, Funding acquisition. **S. Guessasma:** Conceptualization, Validation, Formal analysis, Investigation, Writing – review & editing, Visualization, Supervision, Project administration. **J.**

Beaugrand: Conceptualization, Validation, Investigation, Writing – review & editing, Visualization, Supervision, Project administration, Funding acquisition.

Declaration of Competing Interests

The authors declare that they have no known competing financial interests or personal relationships that could have appeared to influence the work reported in this paper.

Acknowledgments

The authors would like to thank IUT Nantes for the access to their laser cutting machine and Eugène Drouet (INRAE, Nantes) for its help in adapting the tensile testing machine to the SOLEIL environment. We also acknowledge SOLEIL for provision of synchrotron radiation facilities (project 20190747) and Pierre Ouagne and Marie Gregoire from ENIT Tarbes for the access to the pilot scutching line.

References

[1] A. Bourmaud, J. Beaugrand, D.U. Shah, V. Placet, C Baley, Towards the design of high-performance plant fibre composites, Prog. Mater. Sci 97 (2018) 347–408.
[2] C. Chen, Y. Kuang, S. Zhu, I. Burgert, T. Keplinger, A. Gong, et al., Structure–property–function relationships of natural and engineered wood, Nat. Rev. Mater 5 (2020) 642–666.
[3] K. Charlet, J.P. Jernot, S. Eve, M. Gomina, J. Bréard, Multi-scale morphological characterisation of flax: from the stem to the fibrils, Carbohydr. Polym 82 (1) (2010) 54–61.
[4] Müssig J. Industrial Applications of Natural Fibres: Structure, Properties and Technical Applications: Wiley; 2010.
[5] A. Melelli, O. Arnould, J. Beaugrand, A. Bourmaud, The middle lamella of plant fibers used as composite reinforcement: investigation by atomic force microscopy, Molecules 25 (3) (2020).
[6] K. Charlet, A. Béakou, Mechanical properties of interfaces within a flax bundle – part I: experimental analysis, Int. J. Adhes. Adhes. 31 (8) (2011) 875–881.
[7] C. Rihouey, F. Paynel, T. Gorshkova, C. Morvan, Flax fibers: assessing the non-cellulosic polysaccharides and an approach to supramolecular design of the cell wall, Cellulose 24 (5) (2017) 1985–2001.
[8] B. Clair, A. Déjardin, G. Pilate, T. Alméras, Is the G-layer a tertiary cell wall? Front. Plant Sci 9 (2018) 1–4.
[9] T. Gorshkova, T. Chernova, N. Mokshina, M.V. Ageeva, P. Mikshina, Plant 'muscles': fibers with a tertiary cell wall, New Phytol. 218 (2018) 66–72.
[10] A. Melelli, F. Jamme, D. Legland, J. Beaugrand, A. Bourmaud, Microfibril angle of elementary flax fibres investigated with polarised second harmonic generation microscopy, Ind. Crops Prod 156 (112847) (2020) 1–10.
[11] C. Goudenhooft, D. Siniscalco, O. Arnould, A. Bourmaud, O. Sire, T. Gorshkova, et al., Investigation of the mechanical properties of flax cell walls during plant development: the relation between performance and cell wall structure, Fibers 6 (1) (2018).
[12] E. Richely, S. Durand, A. Melelli, A. Kao, A. Magueresse, H. Dhakal, et al., Novel insight into the intricate shape of flax fibre lumen, Fibers 9 (4) (2021).
[13] E. Richely, A. Bourmaud, V. Placet, S. Guessasma, J. Beaugrand, A critical review of the ultrastructure, mechanics and modelling of flax fibres and their defects, Prog. Mater. Sci 124 (100851) (2021) 1–31.
[14] A. Bourmaud, D. Siniscalco, L. Foucat, C. Goudenhooft, X. Falourd, B. Pontoire, et al., Evolution of flax cell wall ultrastructure and mechanical properties during the retting step, Carbohydr. Polym 206 (2019) 48–56.
[15] L. Donaldson, Cellulose microfibril aggregates and their size variation with cell wall type, Wood Sci. Technol. 41 (5) (2007) 443–460.
[16] S.H. Kim, C.M. Lee, K Kafle, Characterization of crystalline cellulose in biomass: basic principles, applications, and limitations of XRD, NMR, IR, Raman, and SFG, Korean J. Chem. Eng. 30 (12) (2013) 2127–2141.
[17] A. Melelli, S. Durand, O. Arnould, E. Richely, S. Guessasma, F. Jamme, et al., Extensive investigation of the ultrastructure of kink-bands in flax fibres, Ind. Crops Prod 164 (2021).
[18] V. Placet, A. Bouali, C. Garcin, J. Cote, P. Perre, Suivi Par DRX Des Réarrangements Microstructuraux Induits Par Sollicitations Mécaniques Dans Les Fibres Végétales Tirées Du Chanvre, 20ème Congrès Français de Mécanique, Besançon, France, 2011.
[19] M.-P. Sarén, R. Serimaa, Determination of microfibril angle distribution by X-ray diffraction, Wood Sci. Technol. 40 (6) (2005) 445–460.
[20] L.A. Donaldson, Microfibril angle: measurement, variation and relationships – a review, Iawa 29 (2008) 345–386.
[21] M. Müller, C. Czihak, G. Vogl, P. Fratzl, H. Schober, C. Rieke, Direct observation of microfibril arrangement in a single native cellulose fiber by microbeam small-Angle X-ray scattering, Macromolecules 31 (1998) 3953–3957.
[22] A. Bourmaud, C. Morvan, A. Bouali, V. Placet, P. Perré, C. Baley, Relationships between micro-fibrillar angle, mechanical properties and biochemical composition of flax fibers, Ind. Crops Prod 44 (2013) 343–351.
[23] C. Wang, N. Wang, S. Liu, L. Choo-Simth, H. Zhang, Z. Zhi, Investigation of microfibril angle of flax fibers using X-Ray diffraction and scanning electron microscopy, J. Nat. Fibers 17 (7) (2018) 1001–1010.
[24] O. Astley, A. Donald, A small-angle X-ray scattering study of the effect of hydration on the microstructure of flax fibers, Biomacromolecules 2 (2001) 672–680.
[25] M. Eder, O. Arnould, J.W.C. Dunlop, J. Hornatowska, L. Salmén, Experimental micromechanical characterisation of wood cell walls, Wood Sci. Technol. 47 (1) (2012) 163–182.
[26] V. Placet, O. Cissé, M. Lamine Boubakar, Nonlinear tensile behaviour of elementary hemp fibres. Part I: investigation of the possible origins using repeated progressive loading with in situ microscopic observations, Compos., Part A 56 (2014) 319–327.
[27] C. Baley, Analysis of the flax fibres tensile behaviour and analysis of the tensile stiffness increase, Compos., Part A 33 (2002) 939–948.
[28] J. Keckes, I. Burgert, K. Fruhmann, M. Muller, K. Kolln, M. Hamilton, et al., Cell-wall recovery after irreversible deformation of wood, Nat. Mater 2 (12) (2003) 810–814.
[29] K.J. Martinschitz, P. Boesecke, C.J. Garvey, W. Gindl, J. Keckes, Changes in microfibril angle in cyclically deformed dry coir fibers studied by in-situ synchrotron X-ray diffraction, J. Mater. Sci 43 (1) (2006) 350–356.
[30] O. Astley, A. Donald, The tensile deformation of flax fibres as studied by X-ray scattering, J. Mater. Sci 38 (2003) 165–171.
[31] K. Kölln, I. Grotkopp, M. Burghammer, S.V. Roth, S.S. Funari, M. Dommach, et al., Mechanical properties of cellulose fibres and wood. Orientational aspects in situ investigated with synchrotron radiation, J. Synchrotron. Radiat 12 (2005) 739–744.
[32] A.P. Wilkins, The nomenclature of cell wall deformations, Wood Sci. Technol. 20 (1986) 97–109.
[33] L.G. Thygesen, M.R. Asgharipour, The effects of growth and storage conditions on dislocations in hemp fibres, J. Mater. Sci 43 (10) (2008) 3670–3673.
[34] A. Hernandez-Estrada, H.-J. Gusovius, J. Müssig, M. Hughes, Assessing the susceptibility of hemp fibre to the formation of dislocations during processing, Ind. Crops Prod 85 (2016) 382–388.
[35] L. Kozlova, A. Petrova, A. Chernyad'ev, V. Salnikov, T Gorshkova, On the origin of bast fiber dislocations in flax, Ind. Crops Prod (2022) 176.
[36] A. Bourmaud, L. Pinsard, E. Guillou, E. De Luycker, M. Fazzini, J. Perrin, et al., Elucidating the formation of structural defects in flax fibres through synchrotron X-ray phase-contrast microtomography, Ind. Crops Prod (2022) 184.
[37] M. Müller, C. Czihak, M. Burghammer, C. Riekel, Combined X–ray microbeam small–angle scattering and fibre diffraction experiments on single native cellulose fibres, J. Appl. Crystallogr 33 (2000) 817–819.
[38] A. Bergander, L. Salmen, Cell wall properties and their effects on the mechanical properties of fibers, J. Mater. Sci 37 (2002) 151–156.
[39] J. Gassan, A. Chate, A.K. Bledzki, Calculation of elastic properties of natural fibers, J. Mater. Sci 36 (2001) 3715–3720.
[40] A. Del Masto, F. Trivaudey, V. Guicheret-Retel, V. Placet, L. Boubakar, Nonlinear tensile behaviour of elementary hemp fibres: a numerical investigation of the relationships between 3D geometry and tensile behaviour, J. Mater. Sci 52 (2017) 6591–6610.
[41] A. Thuault, J. Bazin, S. Eve, J. Bréard, M Gomina, Numerical study of the influence of structural and mechanical parameters on the tensile mechanical behaviour of flax fibres, J. Ind. Text. 44 (2013) 22–39.
[42] M. Sedighi-Gilani, P. Navi, Experimental observations and micromechanical modeling of successive-damaging phenomenon in wood cells' tensile behavior, Wood Sci. Technol. 41 (1) (2006) 69–85.
[43] Trivaudey F., Placet V. Influence de l'Angle des MicroFibrilles (AMF) sur le module d'élasticité longitudinal des fibres végétales – Approche numérique. JST AMAC – Matériaux composites renforcés par des fibres végétales. Lorient 2010.
[44] F. Trivaudey, V. Placet, V. Guicheret-Retel, M.L. Boubakar, Nonlinear tensile behaviour of elementary hemp fibres. Part II: modelling using an anisotropic viscoelastic constitutive law in a material rotating frame, Compos., Part A 68 (2015) 346–355.
[45] T. Nilsson, P.J. Gustafsson, Influence of dislocations and plasticity on the tensile behaviour of flax and hemp fibres, Compos., Part A 38 (7) (2007) 1722–1728.
[46] Q. Deng, S. Li, Y Chen, Mechanical properties and failure mechanism of wood cell wall layers, Comput. Mater. Sci. 62 (2012) 221–226.
[47] A. Khodayari, A.W. Van Vuure, U. Hirn, D. Seveno, Tensile behaviour of dislocated/crystalline cellulose fibrils at the nano scale, Carbohydr. Polym 235 (2020), 115946.
[48] A. Khodayari, U. Hirn, A.W. Van Vuure, D. Seveno, Inverse rule of mixtures at the nanoscale: prediction of elastic properties of cellulose nanofibrils, Compos., Part A (2020).
[49] J. Müssig, K. Haag, The use of flax fibres as reinforcements in composites. Biofiber Reinforcements in Composite Materials, 2015, pp. 35–85.
[50] E. Richely, Combined Experimental End Numerical Approaches to Understand the Structure-Mechanical Property Relationship of Flax Fibres and Bundles, University of Nantes, Nantes, France, 2021. PhD Thesis.
[51] L.G. Thygesen, P. Hoffmeyer, Image analysis for the quantification of dislocations in hemp fibres, Ind. Crops Prod 21 (2) (2005) 173–184.
[52] D.E. Turek, On the tensile testing of high modulus polymers and the compliance correction, Polym. Eng. Sci. 33 (6) (1993) 328–333.
[53] A. Lefeuvre, A. Bourmaud, C. Morvan, C. Baley, Tensile properties of elementary fibres of flax and glass: analysis of reproducibility and scattering, Mater. Lett 130 (2014) 289–291.
[54] K. Desjardins, M. Pomorski, T. Bizien, A. Thureau, C. Menneglier, J. Pérez, An active x-ray beamstop based on single crystal CVD diamond at beamline SWING, Rev. Sci. Instrum. 92 (4) (2021).

[55] M. Müller, B. Murphy, M. Burghammer, C. Riekel, E. Pantos, J. Gunneweg, Ageing of native cellulose fibres under archaeological conditions: textiles from the Dead Sea region studied using synchrotron X-ray microdiffraction, Appl. Phys. A 89 (4) (2007) 877–881.
[56] M. Müller, B. Murphy, M. Burghammer, C. Riekel, M. Roberts, M. Papiz, et al., Identification of ancient textile fibres from Khirbet Qumran caves using synchrotron radiation microbeam diffraction, Spectrochim. Acta Part B 59 (10–11) (2004) 1669–1674.
[57] I.D. Cave, Theory of X-ray measurement of microfibril angle in wood, part 1. The condition for reflection X-ray diffraction by materials with fibre type symmetry, Wood Sci. Technol. 31 (1997) 143–152.
[58] E. Richely, A. Bourmaud, H. Dhakal, Z. Zhang, J. Beaugrand, S. Guessasma, Exploring the morphology of flax fibres by X-ray microtomography and the related mechanical response by numerical modelling, Compos., Part A (2022) 160.
[59] V. Placet, F. Trivaudey, O. Cisse, V. Gucheret-Retel, M.L. Boubakar, Diameter dependence of the apparent tensile modulus of hemp fibres: a morphological, structural or ultrastructural effect? Compos., Part A 43 (2) (2012) 275–287.
[60] COMSOL Multiphysics® v. 5.4. Www.Comsol.Com. COMSOL AB, Stockholm, Sweden.
[61] Simpleware™ ScanIP v. S-2021.03. https://www.synopsys.com/simpleware.html . Synopsys, Inc., Mountain View, USA.
[62] C. Baley, A. Bourmaud, Average tensile properties of French elementary flax fibers, Mater. Lett 122 (2014) 159–161.
[63] Thuault A. Approche Multi-Échelle De La Structure Et Du Comportement Mécanique De La Fibre De Lin, PhD thesis: Caen; 2011.
[64] A.A. Griffith, The phenomena of rupture and flow in solids, Philos. Trans. R. Soc. London Series A 221 (1921) 163–198. Containing Papers of a Mathematical of Physical Character.
[65] A. Lefeuvre, A. Bourmaud, C. Morvan, C. Baley, Elementary flax fibre tensile properties: correlation between stress–strain behaviour and fibre composition, Ind. Crops Prod 52 (2014) 762–769.
[66] L.G. Thygesen, M. Eder, I. Burgert, Dislocations in single hemp fibres—investigations into the relationship of structural distortions and tensile properties at the cell wall level, J. Mater. Sci 42 (2) (2007) 558–564.
[67] I. Burgert, K. Frühmann, J. Keckes, P. Fratzl, S. Stanzl-Tschegg, Properties of chemically and mechanically isolated fibres of spruce (Picea abies [L.] Karst.). Part 2: twisting phenomena, Holzforschung 59 (2005) 247–251.
[68] V. Placet, O. Cisse, M.L. Boubakar, Influence of environmental relative humidity on the tensile and rotational behaviour of hemp fibres, J. Mater. Sci 47 (7) (2011) 3435–3446.
[69] M. Eder, S. Stanzl-Tschegg, I. Burgert, The fracture behaviour of single wood fibres is governed by geometrical constraints: in situ ESEM studies on three fibre types, Wood Sci. Technol. 42 (8) (2008) 679–689.
[70] L.G. Thygesen, N. Gierlinger, The molecular structure within dislocations in Cannabis sativa fibres studied by polarised Raman microspectroscopy, J. Struct. Biol. 182 (3) (2013) 219–225.
[71] N.J. Pagano, J.C. Halpin, Tension buckling of anisotropic cylinders, J. Compos. Mater 2 (1968) 154–176.
[72] D.H. Page, F. El-Hosseiny, K. Winkler, Behaviour of single wood fibres under axial tensile strain, Nature 229 (1971) 252–253.
[73] W. He, S. Zhang, X. Wang, Mechanical behaviour of iregular fibers part I: modelling the tensile behaviour of linear elastic fibers, J. Text. Res. (2001) 556–560.
[74] W. He, X. Wang, S. Zhang, Mechanical behaviour of iregular fibers part II: nonlinear tensile behaviour, J. Text. Res. (2001) 939–942.
[75] V. Placet, A. Bouali, P. Perré, The possible role of microfibril angle of hemp fibre during fatigue tests and its determination using wide-angle X-ray diffraction, Matér. Tech 99 (6) (2011) 683–689.